# **Inorganic Chemistry**

pubs.acs.org/IC Article

# Light- and Chemical-Doping-Induced Magnetic Behavior of Eu Molecular Systems

Tijana Rajh,\* Eric Masson,\* Kyaw Zin Latt, Ashton Smith, Alexander M. Brugh, Naveen Dandu, Daniel Trainer, Larry A. Curtiss, Anh T. Ngo, and Saw-Wai Hla

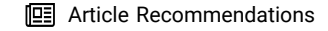


Cite This: Inorg. Chem. 2023, 62, 12721–12729



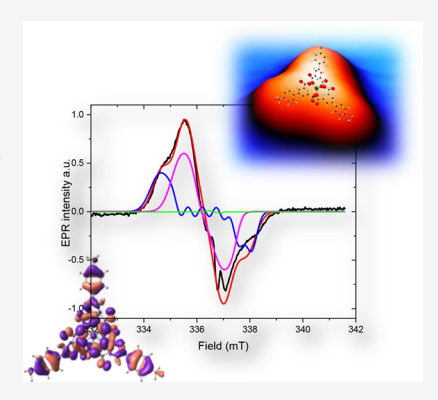
**ACCESS** I

III Metrics & More



s) Supporting Information

**ABSTRACT:** Variable temperature electron paramagnetic resonance (VT-EPR) was used to investigate the role of the environment and oxidation states of several coordinated Eu compounds. We find that while Eu(III) chelating complexes are diamagnetic, simple chemical reduction results in the formation of paramagnetic species. In agreement with the distorted  $D_{3h}$  symmetry of Eu molecular complexes investigated in this study, the EPR spectrum of reduced complexes showed axially symmetric signals ( $g_{\perp} = 2.001$  and  $g_{\parallel} = 1.994$ ) that were successfully simulated with two Eu isotopes with nuclear spin 5/2 ( $^{151}$ Eu and  $^{153}$ Eu with 48% and 52% natural abundance, respectively) and nuclear g-factors  $^{151}$ Eu/ $^{153}$ Eu = 2.27. Illumination of water-soluble complex Eu(dipic) $_3$  at 4 K led to the ligand-to-metal charge transfer (LMCT) that resulted in the formation of Eu(II) in a rhombic environment ( $g_x = 2.006$ ,  $g_y = 1.995$ ,  $g_z = 1.988$ ). The existence of LMCT affects the luminescence of Eu(dipic) $_3$ , and pre-reduction of the complex to Eu(II)(dipic) $_3$  reversibly reduces red luminescence with the appearance of a weak CT blue luminescence. Furthermore, encapsulation of a large portion of the dipic ligand with Cucurbit[7]uril,



Furthermore, encapsulation of a large portion of the dipic ligand with Cucurbit[7]uril, a pumpkin-shaped macrocycle, inhibited ligand-to-metal charge transfer, preventing the formation of Eu(II) upon illumination.

## **■ INTRODUCTION**

Europium (Eu) is a rare-earth metal known as a key element in luminophore development owing to its narrow emission bands and high light purity. It is used as red phosphorus (Eu<sup>3+</sup>) in many different solid-state applications, including upconversion and light-emitting diodes, while high energy broad blue emission of Eu<sup>2+</sup> is used for broad excitation in white lightemitting diodes (W-LED).<sup>3</sup> Eu complexes in liquid solutions are also used in a wide range of applications, with a recent focus on the fluorescent probes in molecular imaging for biology and medicine.<sup>4,5</sup> Europium is unique among the rare earth ions because it has two relatively stable oxidation states that can be easily converted from one to the other; the redox potentials in aqueous solutions are in the range of -0.4 V and −0.8 V vs normal hydrogen electrode (NHE). These redox properties enable simple chemical redox agents to be used for switching between redox states.<sup>6</sup> Because of this, Eu is also proposed as a redox catalyst that can reflect the oxidation state changes during redox-active processes.7

This feature makes europium complexes attractive candidates as redox-sensitive contrasting agents for magnetic resonance imaging (MRI), in which the contrast enhancement generated by these complexes depends on the oxidation state of the metal ion, thereby reporting on the redox properties of its environment. Eu<sup>2+</sup> has a significant magnetic moment resulting in a strong EPR absorption due to seven unpaired electrons in fully occupied half-filled 4f orbitals. This is

particularly important as Eu<sup>2+</sup> is isoelectronic with the most effective MRI relaxing agent gadeolinium,<sup>5</sup> while Eu<sup>3+</sup> is magnetically inactive as it contains a nonmagnetic ground state.<sup>8</sup>

In this study, we explore the magnetic properties of different oxidation states of Eu molecular complexes and assess their conversion from nonmagnetic to paramagnetic states as sensors of their redox environment. We study the magnetic properties of Eu with ligands containing the strongly chelating pyridine-2,6-dicarboxamide (pcam) and dipicolinate (dipic) motifs, enabling Eu to be dissolved in aprotic and protic solvents, respectively. Both ligands form strong complexes with Eu3+9,10 that can be chemically reduced to paramagnetic species with a significant magnetic moment resulting in strong EPR absorption in agreement with seven unpaired electrons of fully occupied half-filled 4f orbitals. Eu<sup>2+</sup> in these molecular chelating complexes has relatively small hyperfine coupling compared to free ions coordinated with solvents due to strong electronic exchange with the ligand. Illumination of Eu(dipic) complexes also results in the formation of Eu<sup>2+</sup>. We employ

Received: April 10, 2023 Published: July 28, 2023





STM studies to obtain structural (imaging) and electronic (dI/dV spectroscopy) parameters of investigated Eu complexes. Using time-dependent density functional theory (TD DFT) calculations, we show that Eu/dipic complexes form a ground state with mixed ligand-to-ligand and metal-to-ligand charge transfer (LLCT/MLCT), while the excited state is indicative of ligand-to-metal charge transfer (LMCT) with the formation of Eu<sup>2+</sup>. Chemically reduced and illuminated Eu(dipic)<sub>3</sub> shows EPR spectra with similar magnetic parameters; however, the axial symmetry of the chemically reduced sample is reduced to rhombic symmetry after illumination. We propose that the symmetry reduction is a consequence of oxidative decarboxylation of the chelating ligand.

## EXPERIMENTAL SECTION

Preparation and Characterization of the Samples. Ligand 1 (as lithium salt) was prepared from chelidamic acid in 3 steps (49% overall yield) after treatment with phosphorus pentabromide followed by in situ esterification of the resulting acyl bromide, Suzuki coupling to *p*-tolylboronic acid, and saponification with lithium hydroxide. Complexes Eu(dipic)<sub>3</sub> and Eu(dipic) (as lithium salts) were prepared quantitatively and selectively (see the SI section for synthetic details and characterization).

X-Band EPR Measurements. CW EPR spectroscopy was acquired with a Bruker ELEXYS E500 spectrometer operating at X-band (9.4 GHz) frequencies equipped with an Oxford ESR900 He flow cryostat with an ITC-5025 temperature controller and a Bruker High QE (HQE) cavity resonator (ER 4122SHQE) at the Center for Nanoscale Materials, Argonne National Laboratory. g tensors were calibrated for accuracy using a known 1,3-bisdiphenylene-2-phenylallyl (BDPA) standard, and the field was calibrated using Mn<sup>2+</sup> in SrO. The CW EPR spectra were collected at 4.2–100 K. If not stated otherwise, the EPR parameters were 0.1 mW microwave power, 2 G modulation amplitude, 100 KHz modulation frequency, and 60 ms conversion time. The simulations were performed by EasySpin using the Eu spin system. <sup>12</sup>

Scanning Tunneling Microscopy (STM). The experiments were performed with a Createc GmbH ultrahigh vacuum (UHV) STM operated at liquid helium temperatures. The Au(111) and Cu[111] single crystal surfaces were used as the supporting substrates were cleaned by cycles of Ne-ion sputtering and annealing. The Eu complexes were deposited on an atomically clean Au(111) substrate between 50 and 300 K substrate temperatures by thermal evaporation under the UHV environment. The sample temperature was then reduced to 5 K for the experiments. Tunneling spectroscopy data were acquired using a lock-in amplifier by adding 20 mV, 725 Hz ac modulation. An electrochemically etched tungsten wire was used as the STM tip, and the tip was further prepared in situ by dipping it into the substrate. The tip quality was checked by determining the well-known Au(111) or Cu(111) surface states prior to each spectroscopic measurement.

DFT and TD-DFT Calculations. In the current work, we first employed first-principles DFT calculations, including range-separated exchange-correlation functional HSE06. 15 We used HSE06 hybrid functional over PBE in VASP to obtain accurate band gaps. To compute optical properties, we utilized PBE1PBE (which is also a hybrid functional) as it is known to accurately reproduce experimental transition energies. 16 Within the HSE06 approach, the value used of exact Hartree-Fock (HF) nonlocal exchange ( $\alpha$ ) was 25%. The screening parameter that controls the extent of the range of the exchange interactions was 0.2. DFT calculations were performed using the Vienna Ab Initio Simulation Package (VASP), which is a plane-wave implementation of DFT. The valence electrons were described in terms of Kohn-Sham (KS) single-electron orbitals, which were expanded in a plane-wave basis with an energy cutoff of 400 eV. Core electrons were defined within the PAW methodology. For the calculations with the HSE06 hybrid functional, we employed a  $\Gamma$ -point- 1  $\times$  1  $\times$  1 k-point mesh. All of the atoms were allowed to

relax until the net force per atom was less than 0.001 eV/Å. We passed the relaxed structure of the complexes for further investigation using time-dependent density-functional theory (TDDFT).<sup>18</sup>

TDDFT calculations based on time-dependent response theory were performed on the optimized geometry of Eu(dipic) complex, using the PBE1PBE $^{19}$  functional with the def2-TZVP $^{20}$  basis set as implemented in Gaussian  $16^{21}$  code to obtain singlet state excited state properties. In our calculations, we computed the first 40 transition excited states.

Natural transition orbitals (NTOs)<sup>22</sup> were calculated to identify the character of the 1st excited state involved in absorption. For this paper, NTOs are obtained by performing unitary transformations of the transition densities as implemented in the Gaussian 1610 software package. Using this method, the highest occupied (HOTO or hole) and lowest unoccupied (LUTO or electron) transition orbital plots at each excited state were obtained. These plots characterize the transitions in the electron densities upon photoexcitation.

Computational Details of Optimizing the Complex Eu(dipic)- $6H_2O \cdot CB[7]^+$  Using GFN2-xTB. First, conformations of Complex  $[Eu(H_2O)_9]^{3+}$  were screened at the semi-empirical GFN2-xTB level<sup>23</sup> in conjunction with the GBSA solvation model for water.<sup>24</sup> Three water molecules were then extruded and replaced by the dipic ligand before subsequent re-optimization with the same method. Finally, the tolyl substituent of the dipic ligand was encapsulated with pre-optimized CB[7], and the complex was re-optimized with the same method.

# ■ RESULTS AND DISCUSSION

Alike to other trivalent rare earth metals, Eu<sup>3+</sup> complexes can be synthesized in square antiprism or trigonal symmetry with a coordination number varying from 6 to 12, with 8 and 9 being the most common. The coordination geometry of Eu<sup>3</sup> depends on the ligand, reaction medium, solvent, and conditions such as the ligand-to-metal ratio. Square antiprism coordination of Eu ions with DOTA macrocycles has been studied most extensively,<sup>25</sup> and in these structures, Eu<sup>3+</sup> ions were found to be coordinated to the four nitrogen atoms of the macrocycle and four oxygen atoms of the pendant arms. 26 In this system, an additional coordination position is occupied by a water molecule which caps Eu<sup>3+</sup> within the macrocycle. Herein, we have synthesized Eu<sup>3+</sup> with tripodal ligands, one ligand that enables trigonal coordination in organic solvents (2,6-pyridine dicarboxamide; pcam), and the other with trigonal coordination in aqueous solution (dipicolinate; dipic). These ligands were chosen because of their strong affinity toward rare earth elements and their well-defined coordination mode in different solvents. 9,27,28

Figure 1 shows structure and STM images of single  $\operatorname{Eu}(\operatorname{dipic})_3$  and  $\operatorname{Eu}(\operatorname{pcam})_3$  complexes deposited on  $\operatorname{Cu}$  and  $\operatorname{Au}$  surfaces, respectively. Clear trigonal coordination of the central  $\operatorname{Eu}$  metal ion with three ligands can be observed. In this coordination, one pyridine nitrogen and two carbonyl oxygen atoms from each ligand coordinate the central  $\operatorname{Eu}$  cation (Figure 1a). This structure results in a distorted  $D_{3h}$  symmetry. The same  $\operatorname{Eu-distorted}$  pseudo-tricapped trigonal prism coordination with pcam ligands was observed using X-ray diffraction, confirming a similar coordination of  $\operatorname{Eu}(\operatorname{pcam})_3$  in solution and on  $\operatorname{Cu}[111]$  substrates (Figure S1).

Eu<sup>3+</sup> is generally EPR-silent due to its nonmagnetic ground state; however, Eu<sup>2+</sup> has a large magnetic moment, resulting in strong EPR absorption caused by its seven unpaired electrons in fully occupied half-filled 4f orbitals. So far, few studies have investigated the structure and paramagnetic properties of Eu<sup>2+</sup> in solution (ammonia,<sup>31</sup> water,<sup>32</sup> and acetonitrile<sup>33</sup>). They

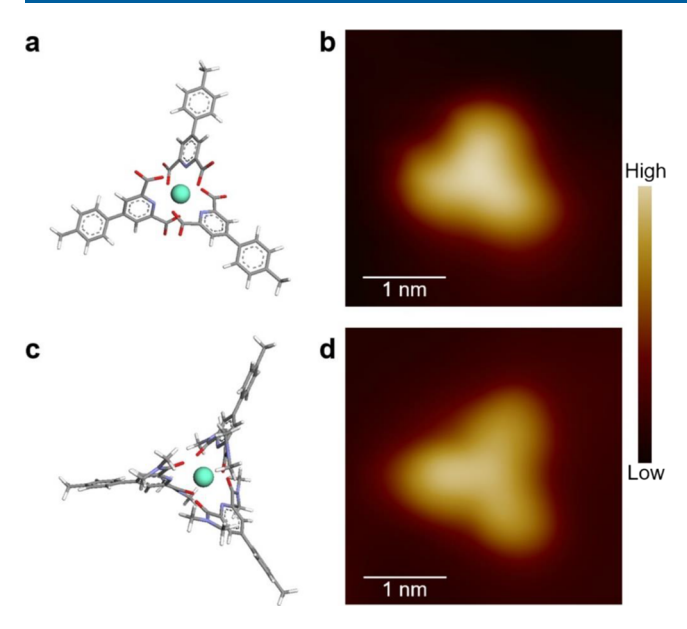


**Figure 1.** Structure of  $Eu(dipic)_3$  and  $Eu(pcam)_3$  complexes (a) a model structure of the  $Eu(dpic)_3$  complex. (b) STM image of  $Eu(dpic)_3$  on Cu(111) at 5 K. [tunneling parameters:  $V_t = 0.2$  V,  $I_t = 0.1$  nA]. (c) Model structure of the  $Eu(pcam)_3$  complex. (d) STM image of  $Eu(pcam)_3$  on  $Eu(pcam)_3$ 

show intense signals at g=1.992 for ammonia-coordinated Eu<sup>2+</sup> and g=1.993 for acetonitrile-coordinated ions, in agreement with Eu<sup>2+</sup> spherically symmetric electronic configuration  $4f^75s^25p^6$  of its ionic state  $^8S_{7/2}$ . Eu<sup>2+</sup> EPR signals also reflect the presence of the nuclear magnetic moment of two Eu isotopes ( $^{151}$ Eu = 47.8% abundant, I = 5/2 and  $^{153}$ Eu = 52.2% abundant, I = 5/2) that provide yet another magnetic probe of the Eu environment via the hyperfine interactions. The hyperfine interaction of Eu<sup>2+</sup> coordinated with ammonia show hyperfine couplings of 35.6 and 15.6 G for  $^{151}$ Eu and  $^{153}$ Eu, respectively, while the hyperfine constants in water and acetonitrile are somewhat larger (37.7 and 16.6 G) for  $^{151}$ Eu and  $^{153}$ Eu, respectively, reflecting contributions of different electronic properties of different coordinating solvents.

We apply variable temperature electron paramagnetic resonance (VT-EPR) to investigate the role of environment on the oxidation states of Eu. We find that while pcam- and dipic-chelated complexes of Eu<sup>3+</sup> are EPR-silent, simple chemical reduction results in the formation of paramagnetic species (Figure 2). Both reduced Eu(dipic)<sub>3</sub> and Eu(pcam)<sub>3</sub> show similar spectra after chemical reduction with reducing agents that are soluble in their respective solvents (sodium borohydride NaBH4 for water and sodium biphenyl for acetonitrile). The EPR spectrum has weak temperature dependence in the 4-77 K range (Figure S2) due to the slow spin relaxation of Eu<sup>2+</sup> Kramer ions with fully occupied half-filled 4f orbitals. The first excited state of Eu half-filled 4f orbitals is at higher energy than other lanthanides, thereby enabling the observation of their EPR features even at room temperature.<sup>34</sup> EPR spectra were successfully simulated with the axially symmetric signal with Lande g-factor  $g_{\perp} = 2.001$ and  $g_{\parallel} = 1.994$  for Eu(dipic)<sub>3</sub> considering natural abundance of Eu isotopes of 48% <sup>151</sup>Eu and 52% <sup>153</sup>Eu, both with nuclear spin 5/2. At the wings of the spectrum, one can recognize the outermost lines of <sup>151</sup>Eu hyperfine sextet (shown in blue in the simulation in Figure 2b) since its nuclear hyperfine constant is

2.27 times larger than that of <sup>153</sup>Eu (shown in magenta in Figure 2b). The center of the spectra is composed of four inner lines of <sup>151</sup>Eu and superimposed with six lines of <sup>153</sup>Eu. However, the absolute value of hyperfine constants reflects a very different coordination environment for chelated Eu complexes compared to free Eu ions in coordinating solvents. <sup>31,33</sup> Hyperfine constants for <sup>151</sup>Eu and <sup>153</sup>Eu used for simulating the spectrum are 6.6 and 2.9 G for dipic and 6.2 and 2.7 G for pcam, respectively, much smaller than hyperfine constants for solvent-coordinated cations.

However, the ratio of hyperfine constants for <sup>151</sup>Eu/<sup>153</sup>Eu remains at 2.27. Small hyperfine constants reflect strong binding of peam and dipic ligands to the central Eu<sup>2+</sup> ion in which the electronic density of Eu is affected by coordinating ligands, thereby reducing the spin density of the central Eu atoms (Table S1).

We also observe the formation of Eu<sup>2+</sup> upon illumination of water-soluble Eu(dipic)<sub>3</sub> at 4 K (Figure 2d). The formation of reduced Eu<sup>2+</sup> upon illumination is unprecedented and is the consequence of the internal redistribution of electronic density within the complex and ligand-to-metal charge transfer (LMCT) at low temperatures. Light-induced LMCT formation between dipic ligands and the Eu<sup>3+</sup> central atom was also confirmed using TD-DFT calculations (Figure 2e). In the ground state of Eu(dipic)<sub>3</sub>, the electronic density indicates the existence of MLCT in both HOMO and LUMO states. In the excited state, the LUMO state gains additional electron density on Eu while the hole becomes delocalized solely on the dipic ligand.

However, EPR spectra of the light-induced excited state show that the symmetry of the Eu<sup>2+</sup> coordination has changed compared to the  $D_{3h}$  crystalline environment ( $g_{\perp}$  = 2.001 and  $g_{\parallel}$  = 1.994) observed in the reduced samples (Figure 2a,b). Instead, we find that Eu<sup>2+</sup> obtained by light excitation is consistent with Eu<sup>2+</sup> in a rhombic environment ( $g_x$  = 2.006,  $g_y$  = 1.995,  $g_z$  = 1.988). The formation of Eu<sup>2+</sup> and its coordination environment are not reversible at 4 K. Illumination of Eu(pcam)<sub>3</sub> does not result in LMCT with the formation of Eu<sup>2+</sup>. These results suggest that the carboxylate groups from the dipicolinate ligand participate in the LMCT and that oxidative decarboxylation<sup>35</sup> of dipic is most probably responsible for the nonreversible symmetry change, which causes departure from the axial symmetry upon illumination (Scheme S2).

We have also investigated the electronic structure of a central Eu<sup>3+</sup> ion using STM by measuring dI/dV tunneling spectra. To distinguish the contribution of the central metal ion and chelating ligands to the LUMO, we have measured dI/ dV tunneling spectra on top of the central Eu ion as well as on the surrounding ligands (Figure 3). Due to the mobility of the molecules on the surface during spectra acquisition, the measurements were performed on an Eu(dipic)<sub>3</sub> complex located next to a counter ion present on the surface. The counter ion was used in these experiments to stabilize the negatively charged Eu(dipic)<sub>3</sub> complex on the Cu(111) surface during the spectroscopic data acquisition, but it does not significantly influence the electronic structure of the complex itself (Figure 3a). Within the measured bias range of  $\pm 2$  V, only LUMO of the Eu(dipic)<sub>3</sub> is observed at ~+1.5 V (Figure 3b). In the dI/dV spectra, the LUMO peak of the central Eu ion reveals a significantly higher intensity as compared to the three surrounding dipic ligands.

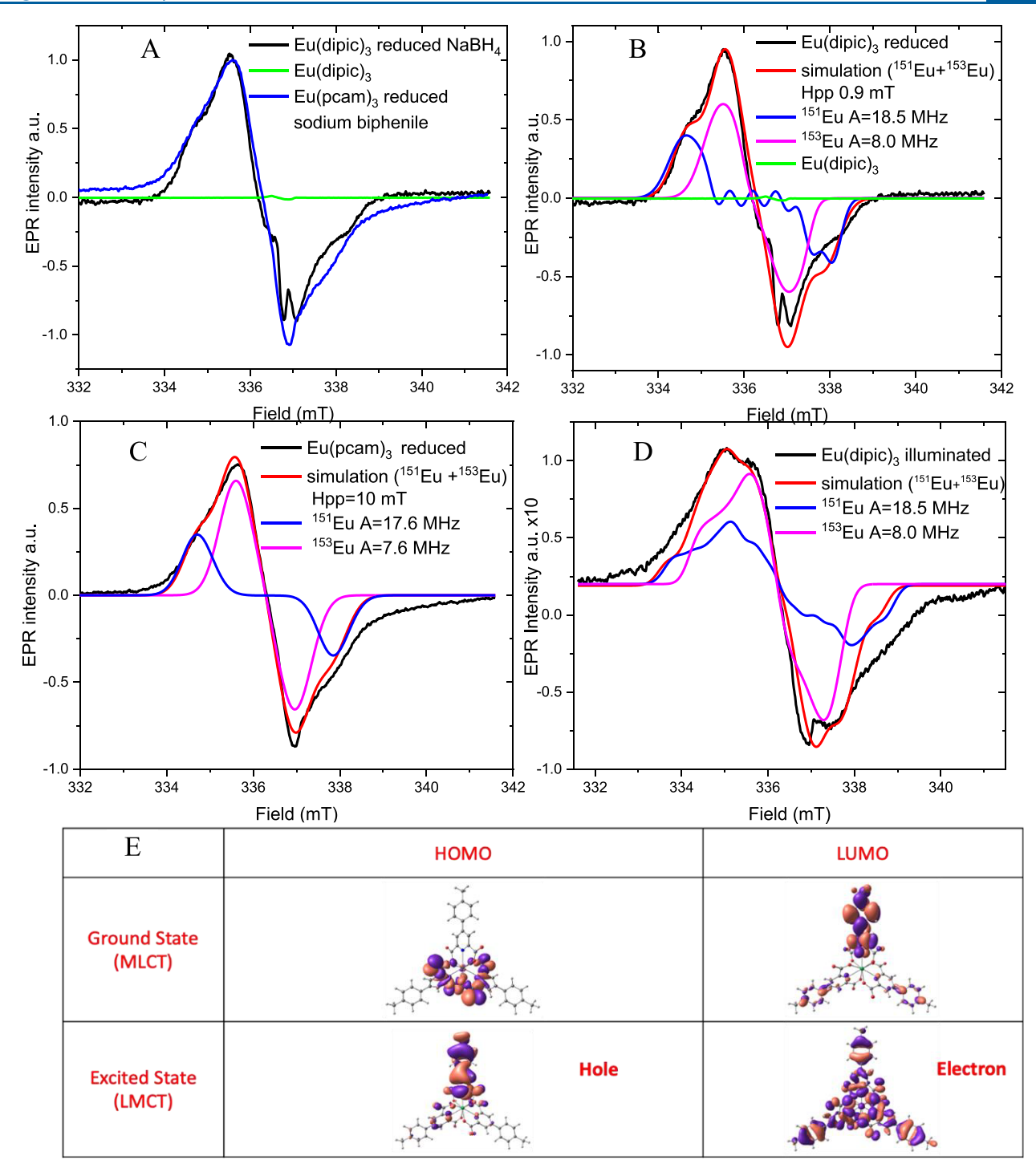


Figure 2. EPR spectra of (A)  $Eu(dipic)_3$  and  $Eu(pcam)_3$  after reduction with NaBH<sub>4</sub> and sodium biphenyl, respectively, in conjunction with their simulations (B) and(C), respectively. Both samples show axially symmetric signal with  $g = [2.001 \ 1.994]$  and  $g = [1.999 \ 1.995]$ , for dipic and pcam, respectively; (D) complex  $Eu(dipic)_3$  after illumination at 4 K exhibits a rhombic spectrum with  $g = [2.006 \ 1.995 \ 1.988]$  and hyperfine coupling of 6.6 G (18.5 MHz) and 2.9 G (8.0 MHz) for <sup>151</sup>Eu and <sup>153</sup>Eu, respectively (same as reduced  $Eu(dipic)_3$ ). (E) TD-DFT calculations of complex  $Eu(dipic)_3$  in its ground state (MLCT) and its excited state (LMCT).

Such intensity differences in LUMO between the Eu ion and the corresponding dipic ligands suggest that the Eu ion has a more considerable affinity toward electrons than the three dipic ligands. The counterion, which is firmly bound to the copper substrate, shows an even smaller electron affinity (Figure 3b). These spectroscopy data are in agreement with EPR results shown in Figure 2a,d that show chemically

reduced and light-induced charge transfer to the central Eu cation and formation of paramagnetic Eu<sup>2+</sup> species.

To probe the contribution of ligand in ligand-to-metal charge transfer states, we have also synthesized a monocoordinated, singly charged 1:1 Eu(dipic) complex that strongly interacts with Cucurbit[7]uril (CB[7]), a pumpkinshape, hollow macrocycle that forms tight complexes with positive amphiphilic guests in water.<sup>36</sup> CB[7] encapsulates the

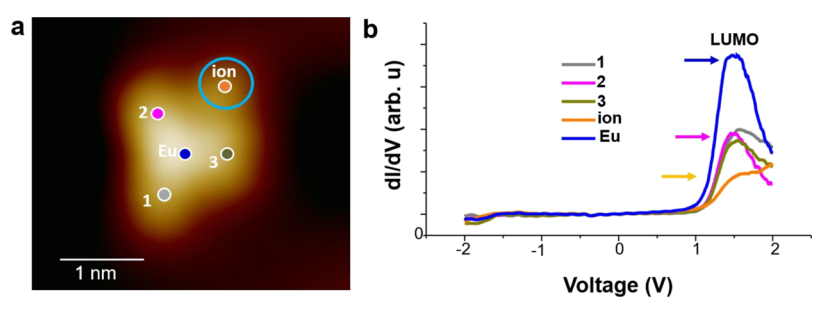


Figure 3. Electronic structure of the Eu(dipic)<sub>3</sub> complex. (a) STM image of Eu-(dipic)<sub>3</sub> complex located next to a counterion (indicated with an oval). (b) dI/dV tunneling spectra correspond to marked locations in (a) [tunneling parameters:  $V_t = -0.2 \text{ V}$ ,  $I_t = 50 \text{ pA}$ ].

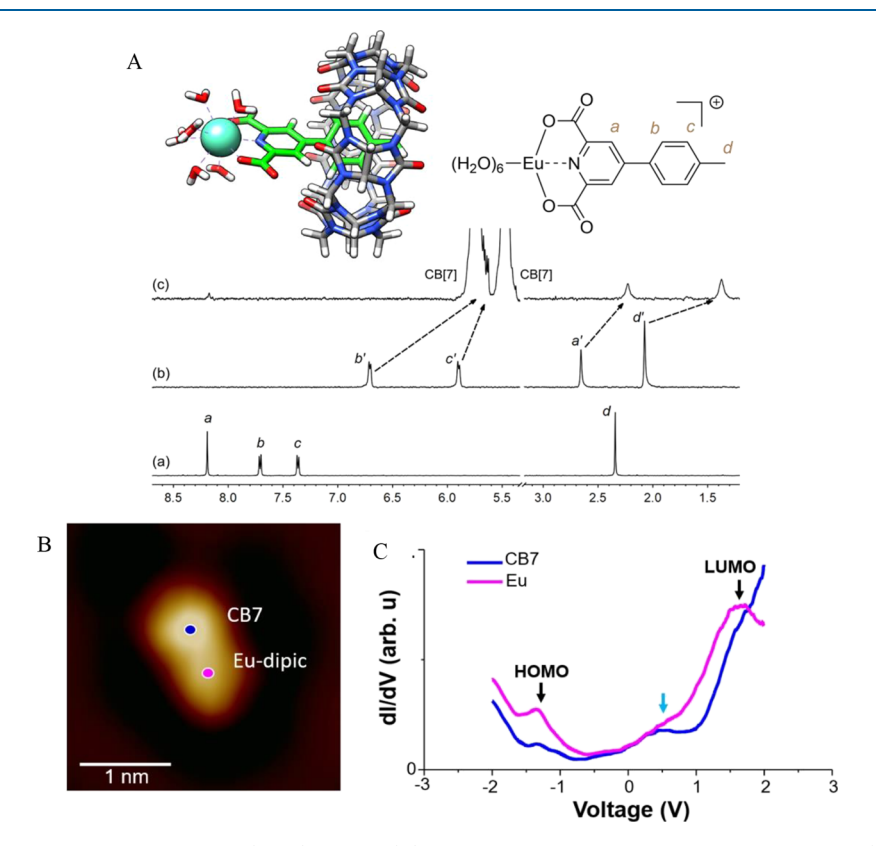


Figure 4. Structural and electronic properties of Eu(dipic)·CB[7]. (A) GFN2-xTB-optimized structure of complex Eu(dipic)· $6H_2O$ ·CB[7]<sup>+</sup>. <sup>1</sup>H-NMR spectra of (a) dipic ligand (1.0 mM), (b) complex Eu(dipic), and (c) complex Eu(dipic)·CB[7] in D<sub>2</sub>O. Chemical shifts in ppm. (B) STM image of complex Eu(dipic)·CB[7] on Cu(111) [tunneling parameters:  $V_t = -0.2 \text{ V}$ ,  $I_t = 0.1 \text{ nA}$ ] in conjunction with (C) dI/dV spectra acquired over CB[7] and Eu(dipic) regions of the complex.

tolyl portion of the dipic ligand with an affinity of  $6.3 \times 10^4$  M<sup>-1</sup>, as obtained by isothermal titration calorimetry (see Figure S16). Tolyl hydrogen nuclei in <sup>1</sup>H-NMR spectra undergo downfield shifts (1.04 and 0.27 ppm for aromatic hydrogens and 0.71 ppm for the methyl group) once encapsulated by CB[7] (see Figure 4a). The number of water molecules q within the first coordination sphere of the Eu<sup>3+</sup> complex in an aqueous solution was calculated using the luminescence lifetimes  $\tau^{-1}$  of the complex in H<sub>2</sub>O and D<sub>2</sub>O and Horrock's formula (see eq 1):<sup>37</sup>

$$q = 1.11(\tau^{-1}_{H_2O} - \tau^{-1}_{D_2O})$$
 (1)

As expected, six water molecules were found to coordinate Eu(dipic) in the absence and presence of CB[7] (luminescence lifetimes  $\tau^{-1}_{\rm H_2O}$  are 0.171 ms in the absence and presence of CB[7];  $\tau^{-1}_{\rm D_2O}$  are 2.61 and 2.02 ms, respectively,

returning q=6.0 and 5.9; see Table S2). Our measured lifetimes in water are in excellent agreement with that published for Eu(2,6-dipicolinate)<sub>3</sub> (0.169 ms).<sup>37</sup> We also note that an ion peak corresponding to complex Eu(dipic)·6H<sub>2</sub>O was observed by electrospray ionization mass spectrometry (see Figure S17).

Figure 5 shows TD-DFT calculations and EPR spectra showcasing the change in the electronic density of Eu(dipic) after light excitation. It was found that similar to the triply coordinated complex (Figure 2), Eu(dipic) undergoes a mixture of LLCT/MLCT in the ground state (Figure 5A, left), making the Eu atom prone to accepting additional electronic density. EPR spectra in Figure 5B confirm that the illumination of 10 mM aqueous solution of complex Eu(dipic) results in the formation of Eu<sup>2+</sup> with very similar magnetic parameters (both electron and nuclear *g*-factors) as the one obtained for Eu(dipic)<sub>3</sub>. In the presence of CB[7], however,

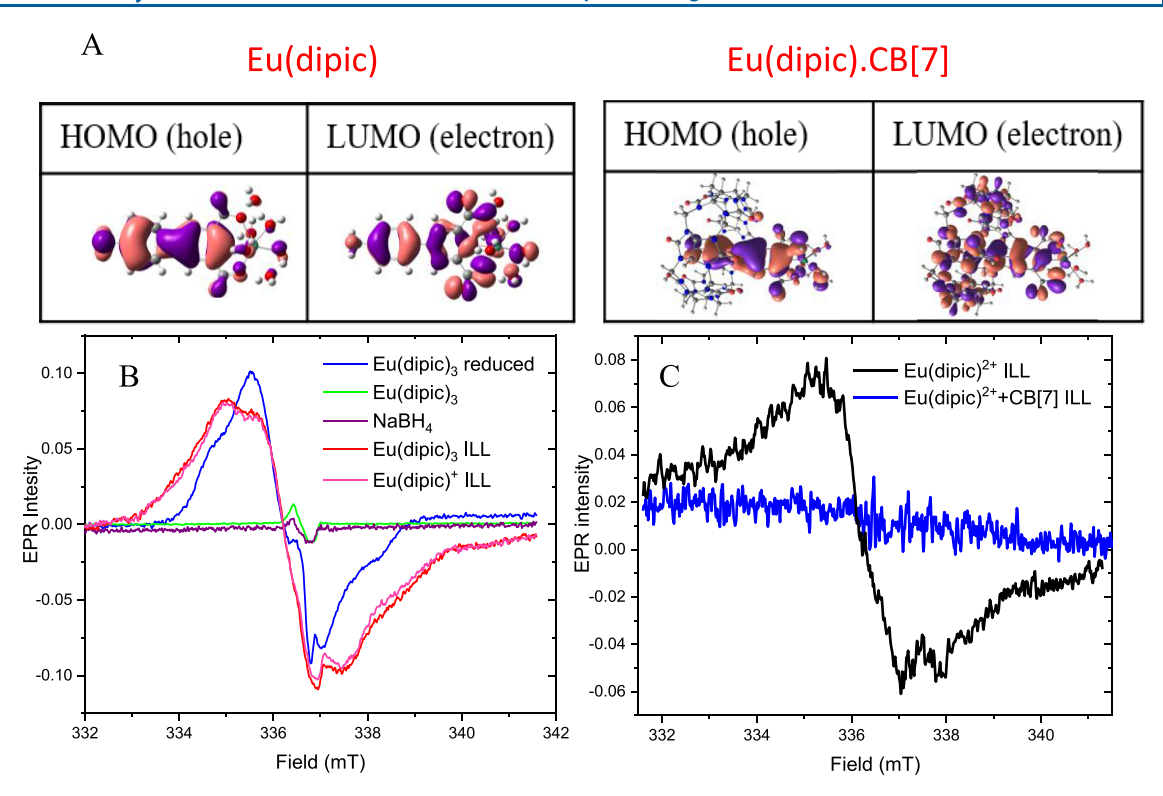


Figure 5. (A) TD-DFT calculations of excited state electronic distribution in  $Eu(dipic) \cdot 6H_2O$  and  $Eu(dipic) \cdot 6H_2O \cdot CB[7]$  showing that upon light excitation, Eu(dipic) undergoes a mixture of LLCT/LMCT. Upon encapsulation into CB[7], light excitation results in the electron density delocalized around the CB[7] macrocycle with no CT to the central Eu ion. (B) EPR spectra of 10 mM  $Eu(dipic)_3$  (red), 10 mM  $Eu(dipic)^+$  (magenta) illuminated for 30 min at 4 K in conjunction with the  $NaBH_4$ -reduced sample (blue). For comparison, the spectra of  $Eu(dipic)_3$  and  $NaBH_4$  reduction with no illumination are also shown. (C) EPR spectra of illuminated 1.0 mM Eu(dipic) (black) and  $Eu(dipic) \cdot CB[7]$  (blue) at 4 K.

the dipic ligand is at least in part encapsulated. TD-DFT calculations show that upon encapsulation, the significant orbital overlap between the dipic ligand and CB[7] orbitals leads to delocalization in the ground state (Figure S18). However, electronic density is redistributed upon excitation to the CB[7] macrocycle rather than the Eu ion (Figure 5A right). This delocalization prevents internal LMCT, which was observed in the free complex, and the exposed Eu does not convert to paramagnetic Eu<sup>2+</sup>. Indeed, EPR shows that while Eu(dipic) undergoes LMCT with the characteristic formation of Eu2+ in a rhombic environment, CB[7] stabilizes the complex, and Eu remains in a nonmagnetic Eu3+ state upon illumination. Figure 5C shows the EPR spectrum of a 1.0 mM solution of Eu(dipic) in water that was illuminated with white light at 4 K for 30 min (black) and the spectrum obtained by illumination of complex Eu(dipic)·CB[7] at 4 K for 30 min (blue). EPR spectra confirm TD-DFT calculations and show that LMCT and oxidative decarboxylation of the dipic ligand is prevented upon CB[7] encapsulation.

An STM image of a single Eu(dipic)·CB[7] complex adsorbed on Cu(111) is shown in Figure 4B. The topology of the complex shows two distinct lobes; the thicker lobe is assigned to the CB[7] macrocycle, while the thinner lobe is associated with hydrated Eu. To determine the energetic positions of frontier orbitals of assembly Eu(dipic)·CB[7], dI/dV tunneling spectra are separately acquired at the Eu ion location and on the CB[7] macrocycle, respectively (Figure 4C). Tunneling spectroscopy data of Eu ions reveal the HOMO and LUMO levels at -1.4 and +1.7 V, respectively, thus revealing a HOMO–LUMO energy gap of 3.1 V. This

value is in a relatively good agreement with projected HOMO–LUMO energy gap obtained by a Gaussian functional of 3.6 eV (Figure S19). The dI/dV spectroscopy reveals that the LUMO of Eu(dipic), +1.7 V, is energetically close to Eu(dipic)<sub>3</sub> (+1.5 V, Figure 3b) and the ability of Eu to receive an electron does not change significantly with CB[7] encapsulation. Moreover, by comparison with the gas-phase electronic structure (Figure S19), we find that the LUMO level has a significant contribution from Eu ion and its energetic position is in agreement with 1.9 eV of the LUMO position of the gas phase molecule.

We find, however, that  $\operatorname{Eu}(\operatorname{dipic})\cdot\operatorname{CB}[7]$  shows a small opposite current at -1.35 V from the HOMO to the support that was not observed in  $\operatorname{Eu}(\operatorname{dipic})_3$  in this bias range, thereby revealing the extra electronic density that is transferred to Eu upon host—guest formation. The calculated density of states confirms the major contribution from the dipic ligand to the HOMO level (Figure S19) but its energetic position, found to be -1.7 V in the gas phase calculations, compared to -1.4 V in dI/dV curve, could indicate weak interaction with the substrate. This additional localized electronic density can also account for the absence of LMCT in the host—guest assembly as observed by EPR spectroscopy.

The existence of light-induced LMCT and oxidation-induced decarboxylation of dipic ligands can also account for a relatively weak luminescence of Eu(dipic). Intercalation of dipic ligand into CB[7], however, further reduces Eu luminescence to half of its intensity, most probably due to the delocalization and excess of dipic electronic density on the Eu site in its HOMO ground state observed in TD-DFT

calculation (Figure S18) and STM measurements. This, in turn, results in a less efficient energy transfer to Eu<sup>3+</sup> as a consequence of the change in the relative position between the energy levels of the blue emitting CT donating state and the Eu  $^5D_2$ ,  $^5D_1$ ,  $^5D_0$  accepting states that lead to red luminescence. Previous studies show that luminescence of Eu complexes with  $\pi$  conjugated dipicolinate ligands proceeds through an intermediate state with a CT character and can be tuned using different  $\pi$ -conjugated dipicolinic acid ligands of the donor group or conjugated backbone. 10 Indeed, luminescence of Eu(dipic)<sub>3</sub> is much stronger than Eu(dipic) but slightly weaker than Eu(pcam)<sub>3</sub> (Figure S20) in solutions and in thin films. Here, we find that pre-reduction of the complex to Eu(II)(dipic)<sub>3</sub> with 1.5 redox equivalent of NaBH<sub>4</sub> drastically reduced photoluminescence intensity of Eu3+ (narrow lines associated with <sup>5</sup>D to <sup>7</sup>F transitions) by 35 times, due to CT state cancellation upon Eu reduction. The luminescence is reversible, and upon oxidation of  $Eu^{2+}$  in  $O_2$ , the luminescence fully recovers to its original intensity. The weak blue luminescence of a CT donating state is not enhanced upon reduction but rather decreased by a factor of 2, confirming that it originates from a CT state rather than reduced Eu<sup>2+</sup>.

In conclusion, we find that chelated Eu complexes show an ability to report on the redox state of their environment due to reversible chemical reduction of the central  $\mathrm{Eu}^{3+}$  ion to  $\mathrm{Eu}^{2+}$ . The reduction is observed both in EPR, with the formation of paramagnetic  $\mathrm{Eu}^{2+}$  and in photoluminescence with removal of the red emission. Paramagnetic  $\mathrm{Eu}^{2+}$  has a large magnetic moment resulting in a strong EPR absorption that is almost temperature-independent in agreement with its seven unpaired electrons in fully occupied half-filled 4f orbitals. Illumination of  $\mathrm{Eu}(\mathrm{dipic})$  and  $\mathrm{Eu}(\mathrm{dipic})_3$  also results in the appearance of paramagnetic complex with the spin density localized on the Eu central ion while the axial symmetry of the paramagnetic complex is lowered to rhombic. Light-induced paramagnetic transition is blocked when ligands are encapsulated into the  $\mathrm{CB}[7]$  macrocyclic host.

### ASSOCIATED CONTENT

### Supporting Information

The Supporting Information is available free of charge at https://pubs.acs.org/doi/10.1021/acs.inorgchem.3c01154.

Details about synthesis and characterization of the Eu complexes; in Eu(dipic) CB[7] ground state and excited state orbitals; EPR of Eu(II)(dipic) $_3$  at different temperatures; absorption and emission spectra of Eu complexes; and their thermodynamic data as well as the decarboxylation mechanism for Eu(dipic) complexes (PDF)

## AUTHOR INFORMATION

## **Corresponding Authors**

Tijana Rajh — School of Molecular Sciences, Arizona State University, Tempe, Arizona 85281, United States; Nanoscience and Technology Division, Argonne National Laboratory, Argonne, Illinois 60540, United States; orcid.org/0000-0003-2218-4130; Email: Tijana.Rajh@asu.edu

Eric Masson – Department of Chemistry, Ohio University, Athens, Ohio 45701, United States; o orcid.org/0000-0001-9387-4783; Email: Masson@ohio.edu

#### Authors

Kyaw Zin Latt – Nanoscience and Technology Division, Argonne National Laboratory, Argonne, Illinois 60540, United States

Ashton Smith – Department of Chemistry, Ohio University, Athens, Ohio 45701, United States

Alexander M. Brugh – School of Molecular Sciences, Arizona State University, Tempe, Arizona 85281, United States

Naveen Dandu – Department of Chemical Engineering, University of Illinois at Chicago, Chicago, Illinois 60608, United States; Materials Science Division, Argonne National Laboratory, Lemont, Illinois 60439, United States

Daniel Trainer – Nanoscience and Technology Division, Argonne National Laboratory, Argonne, Illinois 60540, United States

Larry A. Curtiss — Materials Science Division, Argonne National Laboratory, Lemont, Illinois 60439, United States; orcid.org/0000-0001-8855-8006

Anh T. Ngo — Department of Chemical Engineering, University of Illinois at Chicago, Chicago, Illinois 60608, United States; Materials Science Division, Argonne National Laboratory, Lemont, Illinois 60439, United States

Saw-Wai Hla — Nanoscience and Technology Division, Argonne National Laboratory, Argonne, Illinois 60540, United States; Nanoscale & Quantum Phenomena Institute, and Department of Physics & Astronomy, Ohio University, Athens, Ohio 45701, United States

Complete contact information is available at: https://pubs.acs.org/10.1021/acs.inorgchem.3c01154

### **Author Contributions**

The manuscript was written through contributions of all authors. E.M. and A.S. prepared the samples; T.R. and A.B. performed X-band EPR and fluorescence spectroscopy. K.Z.L., D.T., and S.W.H. performed STM spectroscopy. T.R and A.B. analyzed and simulated EPR spectra. N.D, A.T.N., and L.C. performed DFT calculations. All authors have given approval to the final version of the manuscript.

### Notes

The authors declare no competing financial interest.

# ACKNOWLEDGMENTS

This work was supported by the U.S. Department of Energy, Office of Science, Basic Energy Sciences, Materials Science and Engineering Division. Work performed at the Center for Nanoscale Materials, a U.S. Department of Energy Office of Science User Facility, was supported by the U.S. DOE, Office of Basic Energy Sciences, under Contract No. DE-AC02-06CH11357.

# **■** REFERENCES

- (1) Wen, S.; Zhou, J.; Zheng, K.; Bednarkiewicz, A.; Liu, X.; Jin, D. Advances in highly doped upconversion nanoparticles. *Nat. Commun.* **2018**, *9*, 2415.
- (2) Cardoso, J. P. S.; Correia, M. R.; Vermeersch, R.; Verheij, D.; Jacopin, G.; Pernot, J.; Monteiro, T.; Cardoso, S.; Lorenz, K.; Daudin, B.; Ben Sedrine, N. Europium-Implanted AlN Nanowires for Red Light-Emitting Diodes. *ACS Appl. Nano Mater.* **2022**, *5*, 972–984.
- (3) (a) Wang, L.; Xie, R.-J.; Suehiro, T.; Takeda, T.; Hirosaki, N. Down-Conversion Nitride Materials for Solid State Lighting: Recent Advances and Perspectives. *Chem. Rev.* **2018**, *118*, 1951–2009. (b) Li, J.; Ding, J.; Cao, Y.; Zhou, X.; Ma, B.; Zhao, Z.; Wang, Y. Color-Tunable Phosphor [Mg1.25Si1.25Al2.5]O3N3:Eu2+—A New Modi-

- fied Polymorph of AlON with Double Sites Related Luminescence and Low Thermal Quenching. ACS Appl. Mater. Interfaces 2018, 10, 37307–37315. (c) Dang, P.; Li, G.; Yun, X.; Zhang, Q.; Liu, D.; Lian, H.; Shang, M.; Lin, J. Thermally stable and highly efficient redemitting Eu(3+)-doped Cs(3)GdGe(3)O(9) phosphors for WLEDs: non-concentration quenching and negative thermal expansion. Light: Sci. Appl. 2021, 10, 29.
- (4) (a) Gambino, T.; Valencia, L.; Pérez-Lourido, P.; Esteban-Gómez, D.; Zaiss, M.; Platas-Iglesias, C.; Angelovski, G. Inert macrocyclic <sup>Eu3</sup>+ complex with affirmative paraCEST features. *Inorg. Chem. Front.* **2020**, *7*, 2274–2286. (b) Vashistha, N.; Chandra, A.; Singh, M. HSA functionalized Gd<sub>2</sub>O<sub>3</sub>:Eu<sup>3+</sup> nanoparticles as an MRI contrast agent and a potential luminescent probe for Fe<sup>3+</sup>, Cr<sup>3+</sup>, and Cu<sup>2+</sup> detection in water. *New J. Chem.* **2020**, *44*, 14211–14227.
- (5) Basal, L. A.; Bailey, M. D.; Romero, J.; Ali, M. M.; Kurenbekova, L.; Yustein, J.; Pautler, R. G.; Allen, M. J. Fluorinated Eu(II)-based multimodal contrast agent for temperature- and redox-responsive magnetic resonance imaging. *Chem. Sci.* **2017**, *8*, 8345–8350.
- (6) Burnett, M. E.; Adebesin, B.; Funk, A. M.; Kovacs, Z.; Sherry, A. D.; Ekanger, L. A.; Allen, M. J.; Green, K. N.; Ratnakar, S. J. Electrochemical investigation of the Eu(3+/2+) redox couple in complexes with variable numbers of glycinamide and acetate pendant arms. *Eur. J. Inorg. Chem.* **2017**, 2017, 5001–5005.
- (7) (a) Kim, S.; Kim, Y.; Jin, H.; Park, M. H.; Kim, Y.; Lee, K. M.; Kim, M. Europium-Catalyzed Aerobic Oxidation of Alcohols to Aldehydes/Ketones and Photoluminescence Tracking. *Adv. Synth. Catal.* **2019**, *361*, 1259–1264. (b) Zhang, Y.; Yu, W.-D.; Zhao, C.-F.; Yan, J. Dimensional Reduction of Eu-Based Metal-Organic Framework as Catalysts for Oxidation Catalysis of C(sp3)—H Bond. *Chin. J. Chem.* **2022**, *40*, 480–486. (c) Wang, L.; Zhou, H.; Hu, J.; Huang, B.; Sun, M.; Dong, B.; Zheng, G.; Huang, Y.; Chen, Y.; Li, L.; Xu, Z.; Li, N.; Liu, Z.; Chen, Q.; Sun, L.-D.; Yan, C.-H. A Eu<sup>3+</sup>-Eu<sup>2+</sup> ion redox shuttle imparts operational durability to Pb-I perovskite solar cells. *Science* **2019**, *363*, 265–270.
- (8) Kachkanov, V.; Wallace, M. J.; van der Laan, G.; Dhesi, S. S.; Cavill, S. A.; Fujiwara, Y.; O'Donnell, K. P. Induced magnetic moment of Eu(3+) ions in GaN. *Sci. Rep.* **2012**, *2*, 969.
- (9) Le Borgne, T.; Altmann, P.; André, N.; Bünzli, J.-C. G.; Bernardinelli, G.; Morgantini, P.-Y.; Weber, J.; Piguet, C. Tuning facial—meridional isomerisation in monometallic nine-co-ordinate lanthanide complexes with unsymmetrical tridentate ligands. *Dalton Trans.* **2004**, *5*, 723–733.
- (10) D'Aléo, A.; Picot, A.; Baldeck, P. L.; Andraud, C.; Maury, O. Design of Dipicolinic Acid Ligands for the Two-Photon Sensitized Luminescence of Europium Complexes with Optimized Cross-Sections. *Inorg. Chem.* **2008**, 47, 10269–10279.
- (11) Rosenthal, J.; Yarmus, L. SrO:Mn as EPR Marker and Intensity Standard. Rev. Sci. Instrum. 1966, 37, 381–381.
- (12) Stoll, S.; Schweiger, A. EasySpin, a comprehensive software package for spectral simulation and analysis in EPR. *J. Magn. Reson.* **2006**, *178*, 42–55.
- (13) Hla, S.-W. Scanning tunneling microscopy single atom/molecule manipulation and its application to nanoscience and technology. *J. Vac. Sci. Technol., B* **2005**, *23*, 1351–1360.
- (14) Jäckel, F.; Perera, U. G. E.; Iancu, V.; Braun, K. F.; Koch, N.; Rabe, J. P.; Hla, S. W. Investigating Molecular Charge Transfer Complexes with a Low Temperature Scanning Tunneling Microscope. *Phys. Rev. Lett.* **2008**, *100*, No. 126102.
- (15) Marques, M. A. L.; Vidal, J.; Oliveira, M. J. T.; Reining, L.; Botti, S. Density-based mixing parameter for hybrid functionals. *Phys. Rev. B* **2011**, 83, No. 035119.
- (16) Georgieva, I.; Trendafilova, N.; Zahariev, T.; Danchova, N.; Gutzov, S. Theoretical insight in highly luminescent properties of Eu(III) complex with phenanthroline. *J. Lumin.* **2018**, 202, 192–205. (17) (a) Blöchl, P. E. Projector augmented-wave method. *Phys. Rev. B* **1994**, 50, 17953–17979. (b) Kresse, G.; Furthmüller, J. Efficient iterative schemes for ab initio total-energy calculations using a planewave basis set. *Phys. Rev. B* **1996**, 54, 11169–11186. (c) Kresse, G.;

- Hafner, J. Ab initio molecular dynamics for liquid metals. *Phys. Rev. B* **1993**, 47, 558–561.
- (18) Scalmani, G.; Frisch, M. J.; Mennucci, B.; Tomasi, J.; Cammi, R.; Barone, V. Geometries and properties of excited states in the gas phase and in solution: Theory and application of a time-dependent density functional theory polarizable continuum model. *J. Chem. Phys.* **2006**, *124*, No. 094107.
- (19) (a) Becke, A. D. Density-functional thermochemistry. III. The role of exact exchange. *J. Chem. Phys.* **1993**, *98*, 5648–5652. (b) Lee, C.; Yang, W.; Parr, R. G. Development of the Colle-Salvetti correlation-energy formula into a functional of the electron density. *Phys. Rev. B* **1988**, *37*, 785–789.
- (20) (a) Schuchardt, K. L.; Didier, B. T.; Elsethagen, T.; Sun, L.; Gurumoorthi, V.; Chase, J.; Li, J.; Windus, T. L. Basis Set Exchange: A Community Database for Computational Sciences. *J. Chem. Inf. Model.* **2007**, 47, 1045–1052. (b) Gulde, R.; Pollak, P.; Weigend, F. Error-Balanced Segmented Contracted Basis Sets of Double-ζ to Quadruple-ζ Valence Quality for the Lanthanides. *J. Chem. Theory Comput.* **2012**, *8*, 4062–4068.
- (21) Frisch, M. J.; Trucks, G. W.; Schlegel, H. B.; Scuseria, G. E.; Robb, M. A.; Cheeseman, J. R.; Scalmani, G.; Barone, V.; Petersson, G. A.; Nakatsuji, H.; Li, X.; Caricato, M.; Marenich, A. V.; Bloino, J.; Janesko, B. G.; Gomperts, R.; Mennucci, B.; Hratchian, H. P.; Ortiz, J. V.; Izmaylov, A. F.; Sonnenberg, J. L.; Williams; Ding, F.; Lipparini, F.; Egidi, F.; Goings, J.; Peng, B.; Petrone, A.; Henderson, T.; Ranasinghe, D.; Zakrzewski, V. G.; Gao, J.; Rega, N.; Zheng, G.; Liang, W.; Hada, M.; Ehara, M.; Toyota, K.; Fukuda, R.; Hasegawa, J.; Ishida, M.; Nakajima, T.; Honda, Y.; Kitao, O.; Nakai, H.; Vreven, T.; Throssell, K.; Montgomery, Jr., J. A.; Peralta, J. E.; Ogliaro, F.; Bearpark, M. J.; Heyd, J. J.; Brothers, E. N.; Kudin, K. N.; Staroverov, V. N.; Keith, T. A.; Kobayashi, R.; Normand, J.; Raghavachari, K.; Rendell, A. P.; Burant, J. C.; Iyengar, S. S.; Tomasi, J.; Cossi, M.; Millam, J. M.; Klene, M.; Adamo, C.; Cammi, R.; Ochterski, J. W.; Martin, R. L.; Morokuma, K.; Farkas, O.; Foresman, J. B.; Fox, D. J. Gaussian 16 Rev. C.01; 2016; Gaussian, Inc.: Wallingford, CT (2016) GaussView 5.0. Wallingford, E.U.A.
- (22) Martin, R. L. Natural transition orbitals. J. Chem. Phys. 2003, 118, 4775–4777.
- (23) (a) Grimme, S.; Bannwarth, C.; Shushkov, P. A Robust and Accurate Tight-Binding Quantum Chemical Method for Structures, Vibrational Frequencies, and Noncovalent Interactions of Large Molecular Systems Parametrized for All spd-Block Elements (Z = 1–86). *J. Chem. Theory Comput.* **2017**, *13*, 1989–2009. (b) Bannwarth, C.; Ehlert, S.; Grimme, S. GFN2-xTB—An Accurate and Broadly Parametrized Self-Consistent Tight-Binding Quantum Chemical Method with Multipole Electrostatics and Density-Dependent Dispersion Contributions. *J. Chem. Theory Comput.* **2019**, *15*, 1652–1671. (c) Grimme, S. Exploration of Chemical Compound, Conformer, and Reaction Space with Meta-Dynamics Simulations Based on Tight-Binding Quantum Chemical Calculations. *J. Chem. Theory Comput.* **2019**, *15*, 2847–2862.
- (24) (a) Brieg, M.; Setzler, J.; Albert, S.; Wenzel, W. Generalized Born implicit solvent models for small molecule hydration free energies. *Phys. Chem. Chem. Phys.* **2017**, *19*, 1677–1685. (b) Onufriev, A. V.; Case, D. A. Generalized Born Implicit Solvent Models for Biomolecules. *Annu. Rev. Biophys.* **2019**, *48*, 275–296.
- (25) (a) Ratnakar, S. J.; Viswanathan, S.; Kovacs, Z.; Jindal, A. K.; Green, K. N.; Sherry, A. D. Europium(III) DOTA-tetraamide Complexes as Redox-Active MRI Sensors. *J. Am. Chem. Soc.* **2012**, 134, 5798—5800. (b) Thomsen, M. S.; Madsen, A.; Sørensen, T. J. Crystal structure and optical properties of a two-sited Eu(III) compound: an Eu(III) ion coordinated by two [Eu(III)(DOTA)](—) complexes (DOTA is 1,4,7,10-tetraazacyclododecane-1,4,7,10-tetraacetate). *Acta Crystallogr., C: Struct. Chem.* **2021**, 77, 354—364.
- (26) Blahut, J.; Hermann, P.; Tošner, Z.; Platas-Iglesias, C. A combined NMR and DFT study of conformational dynamics in lanthanide complexes of macrocyclic DOTA-like ligands. *Phys. Chem. Chem. Phys.* **2017**, *19*, 26662–26671.

- (27) Le Borgne, T.; Bénech, J.-M.; Floquet, S.; Bernardinelli, G.; Aliprandini, C.; Bettens, P.; Piguet, C. Monometallic lanthanide complexes with tridentate 2,6-dicarboxamidopyridine ligands. Influence of peripheral substitutions on steric congestion and antenna effect. *Dalton Trans.* 2003, 20, 3856–3868.
- (28) Renaud, F.; Piguet, C.; Bernardinelli, G.; Bünzli, J.-C. G.; Hopfgartner, G. In Search for Mononuclear Helical Lanthanide Building Blocks with Predetermined Properties: Triple-stranded Helical Complexes with N,N,N',N'-tetraethylpyridine-2,6-dicarboxamide. *Chem. Eur. J.* 1997, 3, 1646–1659.
- (29) (a) Andres, J.; Chauvin, A.-S. Colorimetry of Luminescent Lanthanide Complexes. *Molecules* **2020**, 25, 4022. (b) Peters, J. A.; Djanashvili, K.; Geraldes, C. F. G. C.; Platas-Iglesias, C. The chemical consequences of the gradual decrease of the ionic radius along the Lnseries. *Coord. Chem. Rev.* **2020**, 406, No. 213146.
- (30) Li, X.-Z.; Zhou, L.-P.; Yan, L.-L.; Dong, Y.-M.; Bai, Z.-L.; Sun, X.-Q.; Diwu, J.; Wang, S.; Bünzli, J.-C.; Sun, Q.-F. A supramolecular lanthanide separation approach based on multivalent cooperative enhancement of metal ion selectivity. *Nat. Commun.* **2018**, *9*, 547.
- (31) (a) Thompson, D.; Hazen, E.; Waugh, J. Electron Paramagnetic Resonance Study of Solutions of Europium in Liquid Ammonia. *J. Chem. Phys.* **1966**, *44*, 2954–2958. (b) Hsu, S. C. P.; Glaunsinger, W. S. Electron paramagnetic resonance studies of dilute europium-ammonia systems. *J. Phys. Chem.* **1988**, *92*, 1803–1807.
- (32) Caravan, P.; Tóth, É.; Rockenbauer, A.; Merbach, A. E. Nuclear and Electronic Relaxation of Eu<sup>2+</sup>(aq): An Extremely Labile Aqua Ion1. *J. Am. Chem. Soc.* **1999**, *121*, 10403–10409.
- (33) Bodizs, G.; Helm, L. NMR and Electron Paramagnetic Resonance Studies of  $[Gd(CH_3CN)_9]^{3+}$  and  $[Eu(CH_3CN)_9]^{2+}$ : Solvation and Solvent Exchange Dynamics in Anhydrous Acetonitrile. *Inorg. Chem.* **2012**, *51*, 5881–5888.
- (34) McPeak, J. E.; Eaton, S. S.; Eaton, G. R. Electron paramagnetic resonance of lanthanides. In *Methods in Enzymology*; Cotruvo, J. A., Ed.; Academic Press, 2021; vol 651, pp 63–101.
- (35) Nackos, A. N.; Truong, T. V.; Pulsipher, T. C.; Kimball, J. A.; Tolley, H. D.; Robison, R. A.; Bartholomew, C. H.; Lee, M. L. Onestep conversion of dipicolinic acid to its dimethyl ester using monomethyl sulfate salts for GC-MS detection of bacterial endospores. *Anal. Methods* **2011**, *3*, 245–258.
- (36) (a) Liu, S.; Ruspic, C.; Mukhopadhyay, P.; Chakrabarti, S.; Zavalij, P. Y.; Isaacs, L. The Cucurbit[n]uril Family: Prime Components for Self-Sorting Systems. J. Am. Chem. Soc. 2005, 127, 15959-15967. (b) Rekharsky, M. V.; Mori, T.; Yang, C.; Ko, Y. H.; Selvapalam, N.; Kim, H.; Sobransingh, D.; Kaifer, A. E.; Liu, S.; Isaacs, L.; Chen, W.; Moghaddam, S.; Gilson, M. K.; Kim, K.; Inoue, Y. A synthetic host-guest system achieves avidin-biotin affinity by overcoming enthalpy-entropy compensation. Proc. Natl. Acad. Sci. U. S. A. 2007, 104, 20737-20742. (c) Moghaddam, S.; Yang, C.; Rekharsky, M.; Ko, Y. H.; Kim, K.; Inoue, Y.; Gilson, M. K. New Ultrahigh Affinity Host-Guest Complexes of Cucurbit[7]uril with Bicyclo [2.2.2] octane and Adamantane Guests: Thermodynamic Analysis and Evaluation of M2 Affinity Calculations. J. Am. Chem. Soc. 2011, 133, 3570-3581. (d) Cao, L.; Šekutor, M.; Zavalij, P. Y.; Mlinarić-Majerski, K.; Glaser, R.; Isaacs, L. Cucurbit[7]uril Guest Pair with an Attomolar Dissociation Constant. Angew. Chem., Int. Ed. 2014, 53, 988-993. (e) Barbero, H.; Thompson, N. A.; Masson, E. "Dual Layer" Self-Sorting with Cucurbiturils. J. Am. Chem. Soc. 2020,
- (37) Supkowski, R. M.; Horrocks, W. D. On the determination of the number of water molecules, q, coordinated to europium(III) ions in solution from luminescence decay lifetimes. *Inorg. Chim. Acta* **2002**, 340, 44–48.